SCIENTIFIC REPORTS

OPEN

SUBJECT AREAS:
MEMBRANE BIOPHYSICS
PEPTIDES

Received
30 January 2014

Accepted
9 June 2014

Published
27 June 2014

Correspondence and requests for materials should be addressed to M.I.A. (mibel.aguilar@monash.edu)

* These authors contributed equally to this work.

Real-time Measurement of Membrane Conformational States Induced by Antimicrobial Peptides: Balance Between Recovery and Lysis

Kristopher Hall[1]*, Tzong-Hsien Lee[1]*, Adam I. Mechler[2]*, Marcus J. Swann[3] & Marie-Isabel Aguilar[1]

[1]Department of Biochemistry & Molecular Biology, Monash University, Clayton Vic 3800, Australia, [2]School of Molecular Sciences, La Trobe University, Bundoora Vic 3083, Australia, [3]Farfield, Biolin Scientific 3000, Manchester Business Park, Aviator Way, Manchester, M22 5TG, United Kingdom.

The disruption of membranes by antimicrobial peptides is a multi-state process involving significant structural changes in the phospholipid bilayer. However, direct measurement of these membrane structural changes is lacking. We used a combination of dual polarisation interferometry (DPI), surface plasmon resonance spectroscopy (SPR) and atomic force microscopy (AFM) to measure the real-time changes in membrane structure through the measurement of birefringence during the binding of magainin 2 (Mag2) and a highly potent analogue in which Ser[8], Gly[13] and Gly[18] has been replaced with alanine (Mag-A). We show that the membrane bilayer undergoes a series of structural changes upon peptide binding before a critical threshold concentration is reached which triggers a significant membrane disturbance. We also propose a detailed model for antimicrobial peptide action as a function of the degree of bilayer disruption to provide an unprecedented in-depth understanding of the membrane lysis in terms of the interconversion of different membrane conformational states in which there is a balance between recovery and lysis.

The disruption of a membrane by antimicrobial peptides (AMPs) involves a complex sequence of events driven by non-covalent interactions between the peptide and the membrane bilayer which can be described in terms of at least six distinct molecular steps. These include: 1) binding/association to the membrane, 2) conformational change, 3) orientational/topological changes in both peptide and membrane, 4) membrane penetration, 5) peptide self-association, causing irreversible changes in membrane packing and 6) membrane disintegration. Antimicrobial peptide-induced membrane disruption is therefore a dynamic process with structural changes occurring in both the peptide and the membrane bilayer. While many studies also seek to define the mechanism of AMP disruption in terms of either a carpet-like model or a pore-structure[1,2], it is becoming increasingly evident that this "carpet" or "pore" definition is an over-simplification of the lytic process[3–5].

Many studies also define a critical peptide concentration necessary to elicit a lytic response[6]. However, the biophysical definition of the threshold concentration is unclear. While many studies identify a threshold peptide concentration for membrane disruption that may correspond to complete coverage of the vesicle membrane[6], there is also very little information on the relationship between the membrane-bound peptide mass (m_p) and the extent of the concomitant reversible and irreversible changes in the organisation of lipid molecules. Furthermore, defining the final equilibrated structure of the peptide-membrane complex is only part of the mechanism of action of AMPs, as the intermediate paths taken in terms of the conformation and geometry of the membrane bilayer and the peptide, together with the corresponding binding properties (such as membrane binding affinity, kinetics and surface coverage) and the ability to penetrate the outer lipopolysaccharide (LPS) layer (in gram-negative bacteria) all play a role in AMP-membrane interactions that lead to membrane permeabilization. Thus, while the structural changes that antimicrobial peptides undergo during membrane interactions are well understood, much less is known about the structural changes experienced by the membrane or the effect of peptide sequence on bilayer disruption at this critical threshold. The ability to identify and characterise the consecutive stages of the dynamic changes in membrane organization and peptide conformation during the disruption process is therefore critical in defining the mechanism of AMP action. Understanding and enhancing the process of membrane disruption may also open up new avenues for therapeutic intervention targeting bacterial

membrane for drug-resistance infection, which is not currently possible based only on the knowledge of the end-point permeabilization structure.

Magainin 2 (Mag2) is an AMP isolated from the dorsal dermal secretion of the tree frog *Xenopus leavis* with broad spectrum activity against Gram (+) and Gram (−) bacteria and fungi. Its main activity in disrupting membrane function has offered significant potential for combating infections by multi-drug resistant microorganisms. Studies have shown that formation of an amphipathic α-helical structure is important for action[7,8] which may involve the formation of amphipathic toroidal pores[9–14]. However, the exact nature of the peptide-membrane complex remains elusive. Due to the broad antimicrobial activity and low mammalian toxicity of Mag2, a series of mutants have been designed to control structural parameters such as charge density, amphipathicity, hydrophobicity and helicity, with the aim of controlling the selectivity and mechanism of action[15–18]. Among a large number of Mag2 analogues, (Ala[8,13,18])-magainin 2-amide (Mag-A) where Ser[8], Gly[13] and Gly[18] were substituted with alanine, was designed to maximise the helical content while still maintaining an amphipathic structure[19]. Mag-A exhibits enhanced lytic activity and significantly reduced haemolytic activity compared to Mag2[19] and SEM images of *E coli* with the addition of Mag-A showed pronounced wrinkling with bent and elongated morphologies suggesting disruption of membrane integrity[20,21]. While the mechanism of membrane permeabilization by Mag2 and its analogues has been studied on various model membrane systems[11,22–24] and live cells[25], there is limited information on the effect of Mag-A on bilayer structure. We have recently established the use of dual polarisation interferometry (DPI) to characterise the effect of peptide binding on the molecular ordering of the membrane through the measurement of birefringence[4,26–29]. We show here that the membrane bilayer undergoes a series of reversible structural changes upon Mag2 and Mag-A binding before a critical threshold concentration is reached which triggers a significant membrane disturbance. We also propose that this threshold differs from the commonly-defined critical concentration for disruption of the membrane bilayer. Finally, we propose a detailed model for antimicrobial peptide action in terms of the degree of bilayer disruption via interconversion of different membrane conformational states.

Results

Secondary structure of peptides. The sequences and properties of Mag2 and Mag-A are listed in Table S1 and the secondary structures of both peptides in buffer and in the presence of liposomes were determined by circular dichroism (CD) spectroscopy. The CD spectra are shown in Fig S2 and the % helix values are listed in Table S2. The CD spectra showed no defined secondary structure for Mag2 and low helical content for Mag-A in both buffer and in the presence of dimyristoylphosphatidylcholine (DMPC) liposomes (Fig. S2A). By comparison, in the anionic liposomes (containing dimyristoylphosphatidylglycerol DMPG), a significant degree of helical structure was evident for both Mag2 and Mag-A (Fig. S2B, C and D). The addition of cholesterol (chol) or dimyristoylphosphatidylethanolamine (DMPE) caused a decrease in Mag2 helicity but an increase for Mag-A. Overall, the results indicate that the negative charge on the membrane surfaces is important for helix formation of both Mag2 and Mag-A while bilayer structural properties also exert an effect.

Membrane binding characteristics. *Mag2.* The effect of membrane charge and lipid composition on the binding of Mag2 and Mag-A to mammalian membrane mimics DMPC, DMPC/DMPG (4 : 1), DMPC/DMPG/Chol (16 : 4 : 5), and the bacterial membrane mimic DMPE/DMPG (4 : 1) were studied by surface plasmon resonance (SPR). Typical sensorgrams are shown in Fig. 1 and Fig S3. Mag2 binding to DMPC (Fig. 1A) showed a fast initial association that levelled out towards the end of the injection up to a relatively low maximum binding of 450RU at 10 μM, followed by a fast dissociation with around 50% of the peptide remaining bound at each concentration at 600s. Approximately 200RU was retained at 10 μM. At lower concentrations (0.5–4 μM), the association response reached equilibrium faster than at the higher concentrations (6–10 μM).

In contrast to DMPC, Mag2 interaction with anionic DMPC/DMPG (4 : 1) was concentration dependent up to 700RU (Fig 1B), with a small downward slope towards the end of the injection at intermediate concentrations. The interaction with DMPC/DMPG/Chol (16 : 4 : 5) (Fig. S3A) showed similar response profiles to those on DMPC, reaching 650RU at 10 μM. The dissociation of Mag2 from DMPC/DMPG/Chol was slower than from DMPC and DMPC/DMPG lipid layers with 400RU remaining on the surface, corresponding to approximately 60% of material remaining. In contrast, the response of Mag2 on DMPE/DMPG (4 : 1) was much lower, only reaching 300 RU (Fig. S3B), with a very rapid initial association. The dissociation was also fast with about 30% of material still bound.

Mag-A. The level of binding of Mag-A was much higher than Mag2 on all lipids. On DMPC, Mag-A binding reached a maximum of 4000RU (Fig. 1C) which was almost 10 times the Mag2 response (Fig. 1A). The association response was concentration dependent between 0.5–4 μM. However, at 10 μM peptide concentration, after a fast initial association a sharp decrease in response was evident, dropping below the baseline at the end of the injection. The overall drop in response of -3000RU indicated a loss of mass from the DMPC membrane. A similar but less pronounced mass loss was also seen at 8 and 6 μM. The effect on DMPC/DMPG (4 : 1) was similar to that on DMPC but the material loss was even higher (Fig. 1D), already evident at a lower concentrations (3–4 μM) and becoming more substantial with each increase in concentration, with 10 μM showing the greatest effect of -2000RU.

In the presence of cholesterol, the overall effect was similar to Mag2 on the same lipid (Fig. S3C) albeit with a 3–4 times higher response reaching 2000RU at 600s for each concentration, with more than 50% remaining on the surface after rinsing. There was also a small decrease in RU during the association phase, that is, no significant membrane removal occurred. The interaction of Mag-A with DMPE/DMPG (4 : 1) (Fig. S3D) showed similar concentration dependent behaviour to DMPC/DMPG/Chol (16 : 4 : 5), although the response was almost twice as high, reaching 3500RU. The dissociation was slow with similar amounts of material left on the surface at 600s compared to DMPC/DMPG/Chol, with no apparent mass loss.

Peptide Induced Changes in Membrane Order. *Mag2.* Analysis of the changes in the membrane structure upon peptide binding reveals the molecular mechanism of AMP action in terms of surface association, insertion and membrane disruption. The changes in membrane order as a result of peptide binding were quantitatively examined using DPI, through the measurement of optical birefringence (Δn_f) of the bilayer simultaneously with the membrane-bound peptide mass (m_p) in real time. 1.25–40 μM peptide solutions were introduced consecutively to the same lipid bilayer to explore the effect of accumulative exposure of the bilayer surface to each peptide. The values of refractive index (n) and thickness (d) of an adsorbed isotropic single layer are determined by fitting measured phase changes in the transverse electric (T_E) and transverse magnetic (T_M) waveguide modes[4,26,29]. The accumulative binding of Mag2 was first characterised by the TM and TE phase changes as a function of time as shown in Fig 2A and 2B. The TM/TE phase changes increased with increasing Mag2 concentration on DMPC (Fig. 2A). By contrast, an abrupt TM/TE phase loss was observed at 5 μM Mag2 concentration on the DMPC/DMPG bilayer (Fig. 2B). Similar TM/

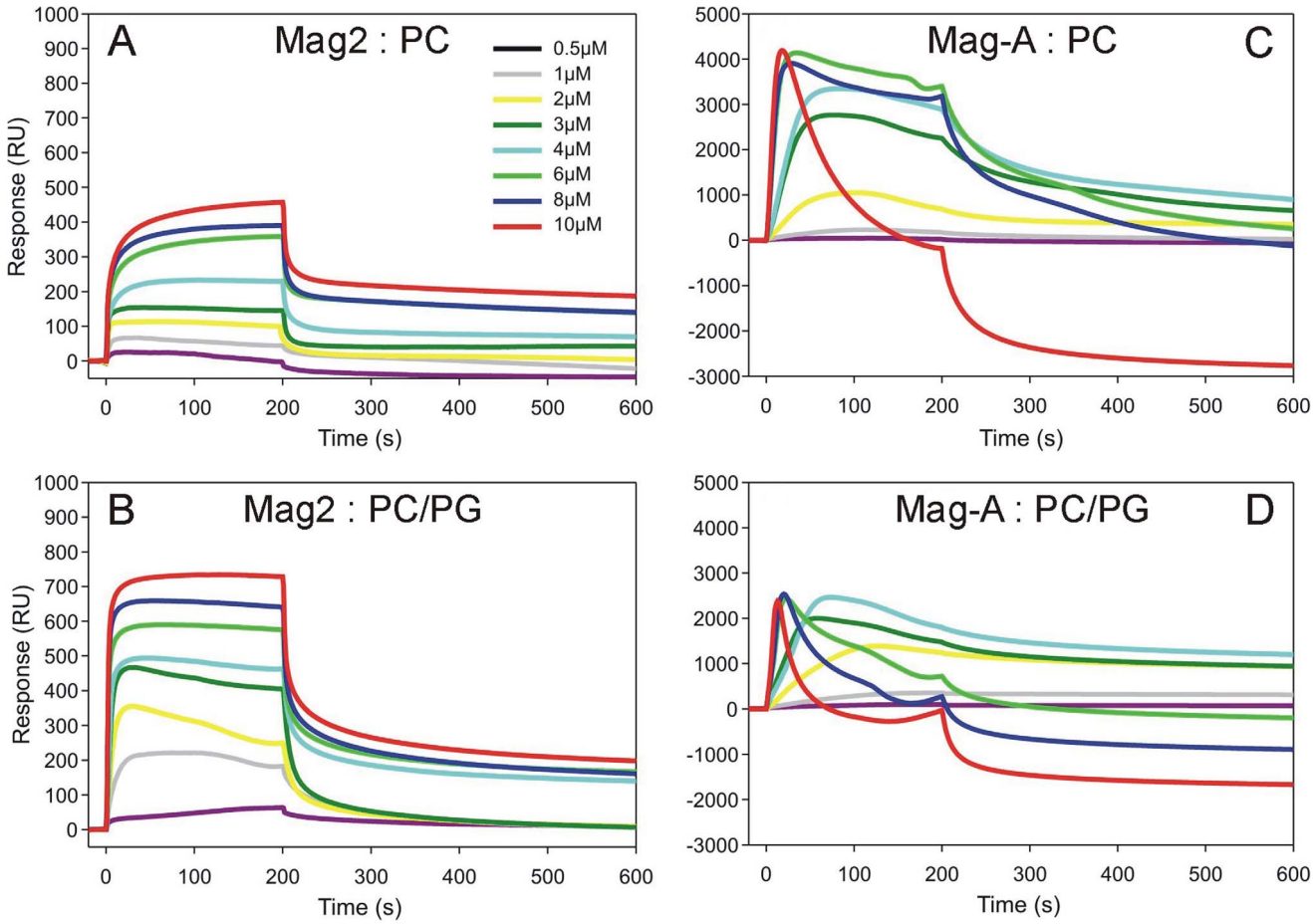

Figure 1 | SPR sensorgrams obtained for Mag2 binding to (A) DMPC and (B) DMPC/DMPG (4 : 1) supported unilamellar bilayers and Mag-A binding to (C) DMPC and (D) DMPC/DMPG (4 : 1) supported unilamellar bilayer at eight different peptide concentrations ranging from 0.5–10 μM. Injections were 200 sec (t = 0–200 sec) at 30 μl/min and the peptide was then allowed to dissociate for a further 400 sec (t = 200–600 sec) as buffer continued to flow through the system.

TE phase changes were observed for Mag-A on both DMPC and DMPC/PG bilayers (Fig. 2C, D).

The measured TM and TE phases were subsequently resolved into the mass of membrane-bound peptide and birefringence for both lipid bilayers[4,26,29]. Plots of mass change versus time and birefringence versus time are shown in Fig. S4. This data was then used to analyse changes in bilayer order as a function of membrane-bound peptide mass (m_p) which allows the impact of peptide binding on the membrane structure to be determined. Specifically, decreases in Δn_f correspond to a decrease in membrane order[4,27,29] and the changes in DMPC and DMPC/DMPG bilayer order induced by Mag2 are shown in Fig. 3A and 3B. As a control, the binding of human coagulation factor IX (known to bind to the surface of PS-containing membranes[30]) to supported POPC/POPE/POPS (3 : 1 : 1) showed no change in the birefringence in spite of a high level of membrane-bound mass (see Fig S5). The injection of 1.25–2.5 μM Mag2 onto the DMPC bilayer (Fig. 3A) did not lead to any significant changes in bilayer order at low m_p. However, 5 and 10 μM Mag2 caused a moderate degree of membrane disordering.

The mass of membrane-bound peptide can be used to derive ratio of the number of peptide to lipid molecules of the upper monolayer, expressed as [P/L]. The [P/L] ratio corresponding to a threshold point at which the birefringence vs m_p plot first exhibits a significant decrease ([P/L]*) was determined to be [P/L]* = 1 : 32 calculated using the upper membrane leaflet (Table S3). The value of Δn_f decreased linearly with further increases in m_p until a minimum Δn_f value was reached where no further change in disorder was observed (indicated by ▲ in Fig 3A). Importantly these decreases in Δn_f were fully reversible during peptide dissociation from the membrane (see dotted arrow). The overall m_p of Mag2 after six accumulated injections was 1.2 ng/mm^2 bound to DMPC while the final Δn_f value was not significantly different to that of the starting bilayer.

Mag2 did not cause any significant changes in the negatively charged DMPC/DMPG bilayer at low peptide concentration (1.25 and 2.5 μM) (Fig 3B). However, when the level of peptide binding reached [P/L]* = 1 : 37 (Table S3), significant disordering was observed which was, however, fully reversible after peptide dissociation. The extent of this disordering then increased linearly with m_p until a further, steeper decrease in Δn_f occurred simultaneously with an irreversible decrease in m_p ([P/L]** = 1 : 15, Table S3), and indicated a major break in membrane packing order. Subsequent increases in Mag2 concentration lead to further large decreases in Δn_f, that is, additional major changes in the membrane packing order, giving rise to a series of parallel lines with each subsequent peptide injection. At the highest concentration of 40 μM Mag2, Δn_f reached a minimum, but significantly, Δn again returned to a value close to that of the starting bilayer after dissociation, in spite of the irreversible decreases in m_p.

Mag-A. The TM/TE phase changes for the binding of Mag-A to the DMPC and DMPC/DMPG bilayers showed pronounced decreases during the injection phase of 5 μM peptide and were similar to the loss in SPR response during the association phase (Fig 2C and D). On

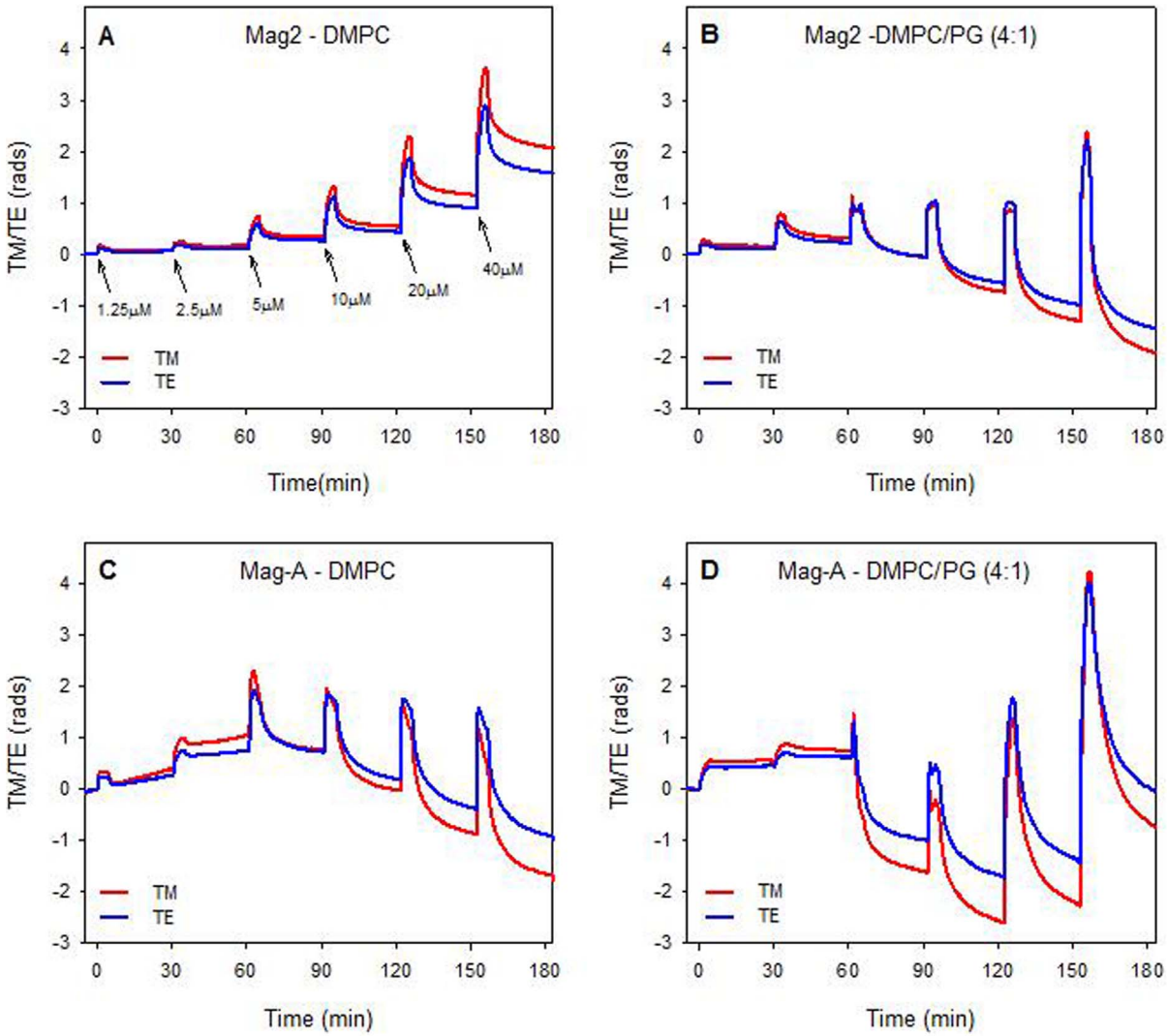

Figure 2 | Real time TM and TE phase changes in radians measured by DPI for Mag2 binding to (A) DMPC and (B) DMPC/DMPG (4 : 1) supported unilamellar bilayers and Mag-A binding to (C) DMPC and (D) DMPC/DMPG (4 : 1) supported unilamellar bilayer. The peptide solutions were injected onto the bilayer accumulatively at concentrations 1.25 μM–40 μM.

DMPC (Fig 3C), Δn_f started to decrease linearly with an increase in m_p ([P/L]* = 1 : 37). At [P/L] = 1 : 8, an abrupt large decrease in birefringence was observed (seen as a major inflection point highlighted in Fig. 3D –marked with **). This large decrease in Δn_f from 0.0195 to 0.0175 with only 0.14 ng/mm^2 drop in mass of bound peptide suggests that the membrane was disrupted without a major loss of material from the surface. Nevertheless the changes in Δn_f were not fully reversible and this partially reversible drop in Δn_f was also observed at 10, 20 and 40 μM Mag-A.

The Δn_f for the interaction of Mag-A to DMPC/DMPG bilayers started to decrease at a very low m_p, and at 1.25 and 2.5 μM the changes in both Δn_f and m_p were almost irreversible. Unlike the linear decrease of Δn_f with m_p observed in DMPC, the Δn_f decrease for DMPC/DMPG was non-linear suggesting that the membrane disorder starts at very low levels of membrane-bound peptide without a clear threshold. However, as the amount of bound peptide reached a [P/L]** = 1 : 13, an overall net loss of mass of about 0.7 ng/mm^2 was observed with decreasing Δn_f during the association phase at 5 μM peptide concentration. A similar but smaller decrease in birefringence was observed at 10 μM. However, a different profile was observed at 20 μM and 40 μM, where the birefringence remained constant with a large increase in mass during the association phase, followed by a significant mass loss during dissociation and a recovery of the remaining bilayer to a Δn_f value similar to that at 5, 10 and 20 μM. These results indicate that the substitution of three residues in Mag2 with alanine causes dramatic changes in both neutral and anionic membrane structure above a specific [P/L] threshold.

Peptide induced changes in membrane morphology. *Mag2.* The changes in the morphology of supported DMPC and DMPC/DMPG (4 : 1) bilayers induced by peptide binding were imaged by atomic force microscopy (AFM). Freshly deposited DMPC liposomes fused into round membrane patches and representative images are shown in Fig. S6. DMPC membranes were typically measured to be 5–6 nm thick (Fig. S6A). 16–21 minutes after the injection of 15 μl of 10 μM Mag2 (capturing an AFM image takes ~ 5 min), the DMPC patch has broken up and small round structures of ~50 nm in diameter with a height of ~5.5 nm were observed (Fig. S6B–D). These round structures leave the surface one by one. By 72 min after injection, a significant proportion of the structures was lost from the surface, and the remaining structures had a much reduced thickness of 2–3 nm (Fig. S6E). Mag2 thus appeared to dissolve the membrane in parts, with sections being lifted off the surface. The DMPC/DMPG liposomes formed a bilayer with a thickness of ~6.0 nm with the appearance of domains differing in height of about 1 nm (Fig. S7).

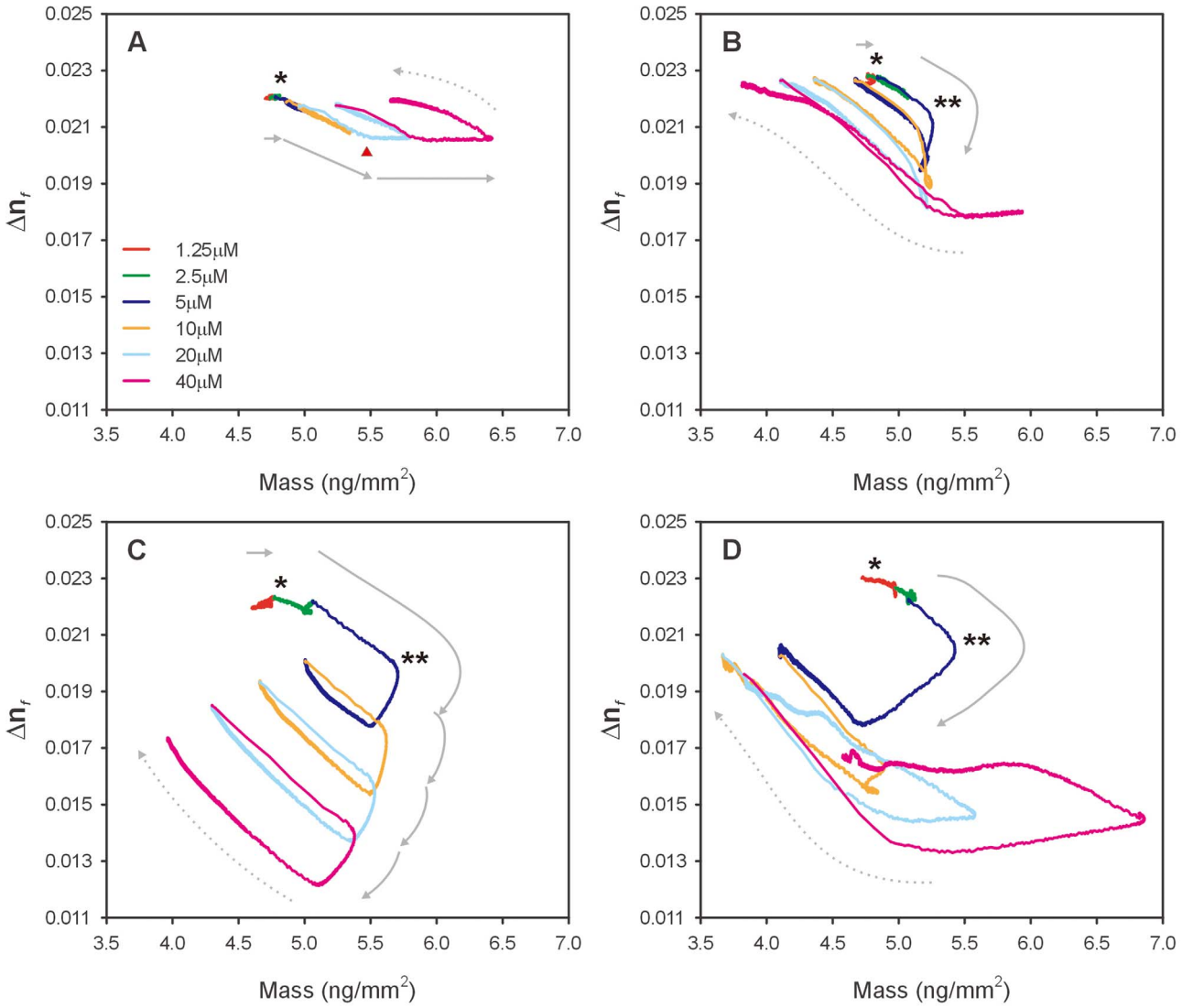

Figure 3 | The effects of Mag2 (A,B) and Mag-A (C,D) on the molecular order of planar DMPC (A,C) and DMPC/DMPG (4 : 1) (B,D) bilayers determined by the optical birefringence as a function of total mass (ng/mm²) of lipid + membrane-bound peptide. The peptides were injected consecutively onto the bilayer with a 2 fold increment in concentration. Solid arrows denote peptide association while dotted arrows correspond to peptide dissociation. ▲ = minimum value observed for Δn_f. * = Δn_f value at initial membrane disordering was observed. ** = Δn_f value at which membrane disruption/mass loss was observed.

After injection of the same amount of Mag2, small holes appeared in the thicker regions of the bilayer, which have also collapsed into a thinner structure. Since the SPR and DPI results show that Mag2 binds more to DMPC/DMPG, the AFM results suggest that these regions may be enriched in DMPG.

Mag-A. The addition of 10 μM Mag-A caused the formation of small defects along the edge of a DMPC bilayer (Fig. S8A and S8B, Video S1) at around 31 min which increased in size at 54 mins (Fig. S8C) together with small holes. The membrane morphology imaged at 72 mins (Fig. S8D) showed that the holes had expanded and that the membrane patches had also expanded, taking up almost the entire 2 × 2 μm image. The cross-sectional measurement showed that the thickness of the membrane layer decreased from 5 nm to 3.5 nm. A similar change in the morphology of DMPC/DMPG (4 : 1) bilayer was observed with small defects at the membrane edges at 20 min and membrane expansion (Fig 5, Video S2). These changes were also associated with the formation of several small depressions and holes at 20–69 min (Fig 4B). After further incubation, the membrane disintegrated into small fragments with significant reduction in layer thickness to ~1.5 nm (Fig. 4C & D). This fragmented membrane spread across most of the mica substrate. These decreases in bilayer thickness and spreading bilayers correspond to a significant disruption of the bilayer and are consistent with the loss in mass/mm² from the surface observed by DPI during the association phase.

Discussion

We have previously demonstrated with DPI and solid state NMR that AMP binding induces discrete changes in bilayer order which correspond to surface binding, partial insertion and full insertion and sometimes membrane loss[4,26,27,29,31]. We hypothesise that there are specific stages in these membrane bilayer changes from which the membrane can either recover or which ultimately proceed to bilayer destruction. Accordingly we propose that the critical concentration corresponds to the point at which the bilayer structure cannot recover. In this study, we have investigated the mechanism of membrane binding of Mag2 and the highly potent analogue Mag-A in order to identify the factors which 1) drive the structural changes in both the membrane and the peptide and 2) define the critical concentration required for membrane lysis.

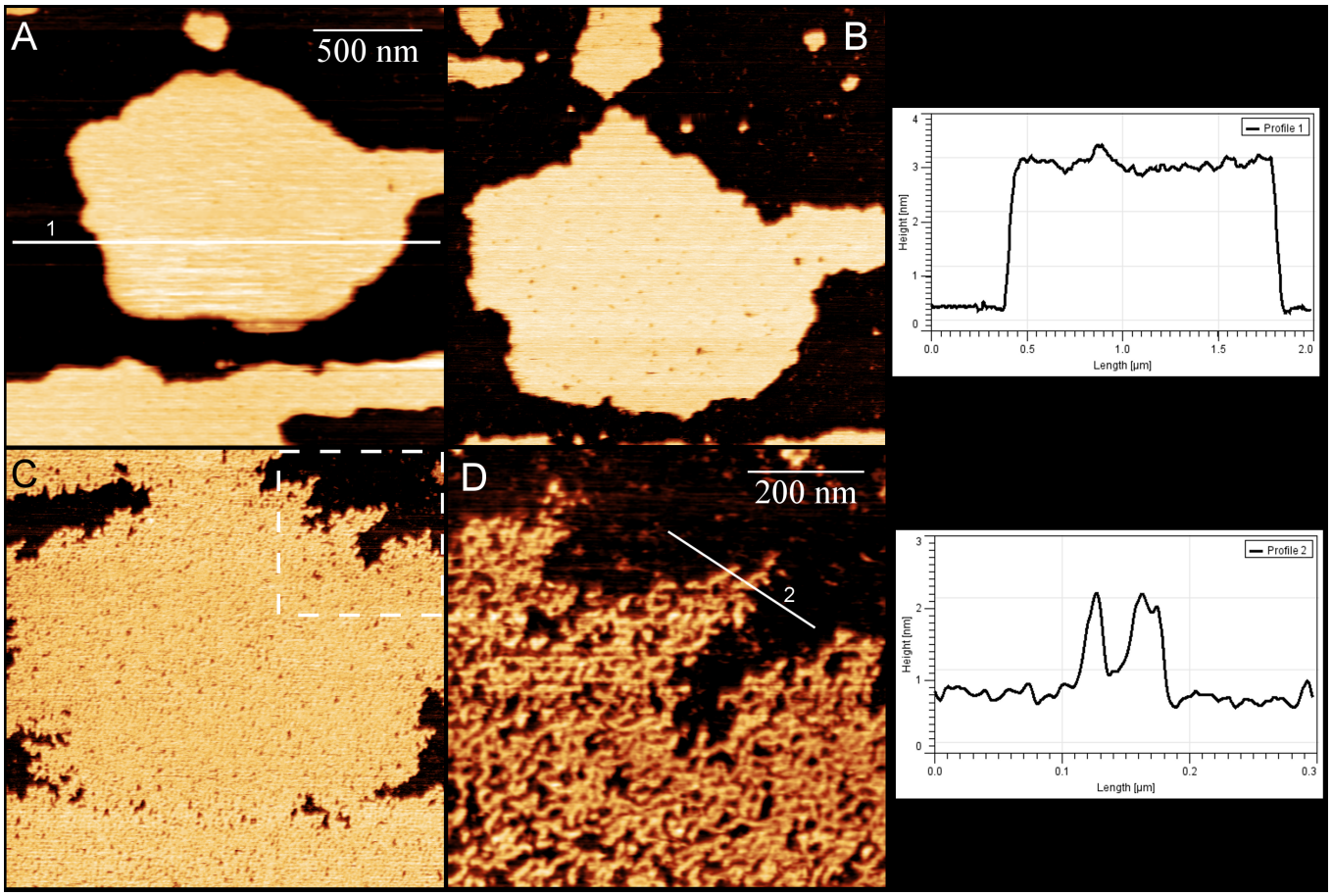

Figure 4 | The sequential changes of supported DMPC/DMPG (4 : 1) bilayer AFM images obtained in real time upon binding of Mag-A. A series of DMPC/DMPG images were taken at (A) in the absence peptide with approximately 3.5 nm in height as shown in the cross-section plot at the top right panel corresponding to the green bar in (A). Images were then taken at (B) 69 minutes and (C) 94 minutes after the injection of Mag-A. The images in (D) showed a high resolution image of the upper right hand area in blue box in (C). A cross section (yellow bar) is shown on the right. Scale bar is 400 nm for (A, B & C) and 150 nm for (D).

We have analyzed the relationship between birefringence (a measure of bilayer order) and the mass of bound peptide (Fig 3). These plots are similar to conventional lipid phase diagrams[32] but reveal the direct effect of bound peptide on membrane structure and the changes in the slope of these plots reveal discrete steps in the binding process. Small changes in the slope $\Delta n_f/m_p$ correspond to surface adsorption of the peptide with little penetration into the membrane, while larger drops in birefringence reveal significant disordering of the bilayer which may correspond to insertion of the peptide into the bilayer[4,26,27,29,31]. A change in the direction of the plot associated with a drop in both birefringence and mass (to give a positive $\Delta n_f/m_p$ value) occurs when there is loss of material from the surface corresponding to disruption of the bilayer structure. Finally, the ability of the bilayer to recover from the disruptive effects of peptide binding is evident from the increase in birefringence after dissociation of the peptide, often returning to the pre-injection value.

Inspection of the different DPI profiles in Fig 3 clearly shows multiple distinct stages in the interaction of Mag2 and Mag-A with phospholipid bilayers. The CD results reveal that Mag2 adopts very little structure in the presence of DMPC, although SPR and DPI reveal some degree of association. The small change in birefringence suggests that it does not insert into the bilayer to any great extent. AFM suggests that these changes in birefringence correspond to destabilisation of the bilayer. Importantly, the bilayer recovers from these changes upon dissociation of Mag2. By comparison, Mag2 adopts a helical structure when binding to the anionic DMPC/DMPG bilayers, while DPI birefringence data indicates that it substantially alters the membrane order, suggesting some degree of membrane penetration as confirmed by AFM, yet the membrane still recovers after each injection.

In contrast, Mag-A adopts partial helical structure in DMPC, binds to the membrane in larger quantities, induces disorder in the bilayer at relatively low concentrations, and causes full disruption and loss of membrane material from the surface over a specific threshold of bound peptide. Moreover, the bilayer that remains on the surface recovers to a significant extent after dissociation at peptide concentrations below the disruption threshold. On the anionic DMPC/DMPG bilayers, Mag-A adopts helical structure, causes substantial disruption of the DMPC/DMPG bilayer from which it cannot recover at higher concentrations and again leads to loss of membrane from the surface. In both cases, AFM shows significant disruption of the lipid bilayer by Mag-A in which holes appear and the bilayer expands. Our results correlate well with previous studies that have demonstrated by ss-NMR that Mag2 and related analogues cause changes in the bilayer structure inducing lipid de-mixing and also phase changes from a lamellar to isotropic or hexagonal phases and membrane thinning[33,34]. Moreover it has been shown by sum frequency generation (SFG) vibrational spectroscopy that Mag2 and the related peptide MSI-78 orient parallel to the membrane surface at low concentrations but insert into the bilayer at higher P/L ratios[35,36].

Overall our studies also demonstrate that a threshold amount of peptide on the membrane surface is necessary after the initial binding-folding processes to promote changes in the membrane structure, followed by a second threshold for membrane lysis. A key

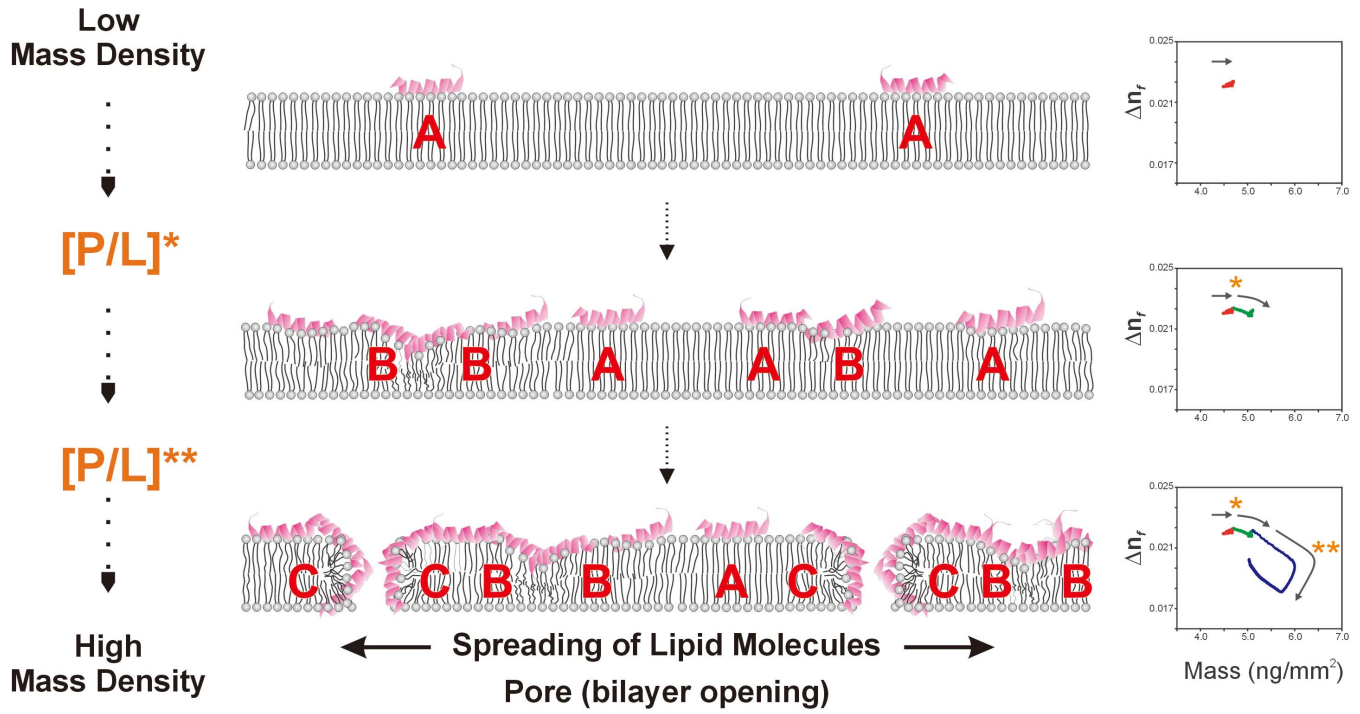

Figure 5 | Schematic showing the interconversion of at least three conformational states of the phospholipid bilayer upon interaction of antimicrobial peptides.

parameter in defining the mechanism of action is the amount of bound peptide required to trigger the irreversible change in membrane structure[1,37]. Our results provide the first evidence in real time that this threshold concentration directly correlates with a change in the membrane structure and packing. Conventionally, the critical peptide concentration is defined as the concentration necessary to cause membrane lysis[6]. In our study, each orientational state corresponding to a significant change in membrane order can be characterised by a specific surface molar threshold ([P/L]), that is, multiple thresholds are evident during the binding process. Significantly, these threshold molar ratios, as we define them, refer to peptide bound to the membrane from the virtually infinite bulk reservoir of the solution phase from which we identified two significant events. Firstly, [P/L]* corresponds to the point at which the initial first drop occurs in the membrane birefringence, while [P/L]** corresponds to the loss of mass from the surface as a result of membrane disruption. For DMPC, both Mag2 and Mag-A induced initial disordering at similar values of [P/L]* = 1/32 and 1/48. For DMPC/DMPG, lower peptide loadings of [P/L]* = 1/37 and 1/69 respectively were necessary to cause the initial bilayer disorder. While Mag2 did not induce significant lysis of DMPC, a [P/L]** of at least 1/8 was required for lysis by Mag-A. Significantly, both peptides caused lysis of the negatively charged DMPC/DMPG at similar values of [P/L]** = 1/13 - 1/15. Thus while the relative affinities of each peptide for DMPC/DMPG are quite different, a similar mass of bound peptide induced bilayer disruption, consistent with P:L ratios reported elsewhere[6].

A very significant outcome of these studies therefore, is the ability to track the changes in membrane structure disorder as a function of mass of bound peptide in real time. In terms of the different structural states adopted by the bilayer, we have previously shown by SS-NMR that the presence of DMPG in DMPC leads to the formation of an isotropic state and that the negative charges on the membrane surface resulted in a greater susceptibility of the bilayer to peptide-induced disordering as measured by DPI[26]. Based on the multiple stages of membrane structure changes evident in Fig. 3, we propose a new model for the molecular mechanism of antimicrobial peptide action in terms of a series of intermediate states, each representing an ensemble of closely-related bilayer structures, as depicted schematically in Fig. 5. Three general membrane-inserted states are proposed which correspond to (A) surface-bound peptide, (B) partially inserted peptide and (C) significantly inserted peptide. This model describes alternate pathways of intermediate membrane states that occur in the presence of increasing amounts of bound peptide and the prevalence of each state is dependent on the peptide and the lipid composition. At low levels of membrane-bound peptide (m_p), State A exists with little bilayer disruption. At higher values of m_p, membrane birefringence decreases reflecting a transition from predominantly A to B at a critical [P/L]* value. Subsequent increases in m_p give rise to State C which is associated with significant disruption and expansion of the bilayer leading to mass loss at a second critical concentration [P/L]**.

This model, based on birefringence changes at critical mass loadings, allows the properties of membrane-active peptides to be analysed in terms of surface binding, insertion, membrane opening and bilayer lysis, and in more detail than has been previously possible in terms of dynamic structural changes. In particular, the molecular events prior to membrane lysis can be fully characterised in terms of bilayer structural changes and provides new criteria that can guide the design of selective antibacterial peptides. Previous studies that have focussed on membrane structural changes have defined two states, the S-state where the peptide is surface bound, and the I-state where the peptide is inserted into the bilayer[1]. More recently, the existence of a 3rd E-state has been proposed where the continued insertion of peptide causes expansion of a pore-like structure[5]. Our results demonstrate the existence of continual changes in bilayer structure during peptide binding and our model defines critical points at which the membrane either recovers or proceeds towards full lysis. Both peptides caused a much greater disruption of DMPC/DMPG than DMPC alone. However, DMPC/DMPG/cholesterol and DMPE/DMPG were both resistant to full lysis by either peptide which has been recently observed by others and related to the influence of these lipids on bilayer rigidity and membrane packing[38–40]. Understanding the process leading to membrane disintegration is at the core of designing selective antimicrobial agents and requires

consideration of the extent of membrane structural changes for a particular peptide. The model presented here therefore provides a detailed mechanism for the membrane structure changes prior to membrane lysis and evidence that quite subtle changes in amino acid structure can modulate the mechanism of insertion, or increase the degree of penetration to an extent that causes lysis. These studies therefore provide a platform for future studies to manipulate the insertion step through changes in peptide structure and selectively prevent the lysis mechanism in host cells while enhancing lytic efficiency in target microbial cells.

Methods

Chemicals and reagents. All chemicals and reagents were purchased from Sigma-Aldrich (St Louis, MO, USA) or Merck (Kilsyth, VIC, Australia). The sequences and physical properties of magainin 2 (Mag2) and (Ala[8,13,18])-magainin 2-amide (Mag-A) are listed in Table S1. Hellmanex II was obtained from Hellma (Müllhein, Germany). Water was quartz-distilled and deionised in a Milli-Q system (Millipore, Bedford, MA, USA). Liposomes were prepared by the extrusion method as described previously[4,29].

Circular Dichroism (CD). CD measurements were carried out on a Jasco J-810 circular dichroism spectropolariser (Jasco, Tokyo Japan) as previously described[29,41] using a peptide to lipid (P/L) molar ratio of 1 : 100 in 20 mM phosphate buffer pH 7.4, 150 mM NaCl.

Surface Plasmon Resonance (SPR). SPR experiments were carried out with a Biacore T100 analytical system on L1 sensor chip (Biacore, Uppsala, Sweden) as previously described[42–46]. A minimum of 5000RU was deposited which corresponds to 5 ng/mm^2. The interaction of Mag2 and Mag-A with DMPC, DMPC/DMPG (4 : 1), DMPC/DMPG/Cholesterol (16 : 4 : 5) and DMPE/DMPG (4 : 1) was examined at peptide concentrations, 0.5, 1, 2, 3, 4, 6, 8 and 10 μM at 25°C, which is above the Tm of the phospholipids. The running buffer was 20 mM phosphate buffer pH 7.4, 150 mM NaCl. Kinetic analysis of the sensorgrams was performed using the langmuir, the parallel and the two state curve fitting models as previously described[46].

Dual Polarisation Interferometry (DPI). DPI provides a quantitative measurement of the optical birefringence of supported lipid bilayer as a function of membrane-bound peptide mass which determines the impact of peptide binding on the molecular order of bilayers[29,47]. The unmodified silicon oxynitride FB80 AnaChips (Farfield-Group, UK) and running buffer, 10 mM MOPS pH 7.0, 150 mM NaCl, were calibrated as previously described[4,29], Following cleaning and calibrating, DMPC and DMPC/DMPG (4 : 1) liposome solution were deposited in the presence of 1 mM $CaCl_2$ at 28°C. The full coverage and quality of membrane was confirmed by the absence of BSA (50 μg/ml) binding[29]. Data was acquired at 10 Hz using *Ana*Light200 version 2.1.0 and analyzed using *Ana*Light® Explorer.

Mag2 and Mag-A were prepared at concentrations of 1.25, 2.5, 5, 10, 20 and 40 μM in 10 mM MOPS, pH 7, 150 mM NaCl. Peptide samples were injected consecutively in an order of 2 fold increment concentration onto the deposited bilayer at 20°C. 160 μl of each peptide concentration was injected at 40 μl/min, followed by running buffer for 30 min prior to injecting the next concentration onto the same bilayer surface. Each peptide concentration measurement was performed on the same lipid bilayer, after which the waveguide surface was regenerated with 2% SDS, 10% Hellmanex II and ethanol at 28°C[29]. The optical birefringence (Δn_f) of each bilayer was determined through calculating the difference between two effective refractive indices, namely the refractive index (RI) of the transverse magnetic (TM) waveguide mode ($\boldsymbol{n}_{TM}$) and the RI of the transverse electric (TE) waveguide mode ($\boldsymbol{n}_{TE}$) as previously described[4,26,27,29,47,48]. An average bilayer thickness of 45.3 ± 0.6Å and a birefringence of 0.0216 ± 0.0005 was obtained for DMPC while an average bilayer thickness of 47.7 ± 1.6 Å and a birefringence of 0.0233 ± 0.0008 was obtained for DMPC/DMPG (4 : 1). dn/dc is the specific refractive index increment of the layer. The de Feijter formula assumes that dn/dc remains constant throughout the experiment. For the present analysis, dn/dc values of 0.135 and 0.182 mL/g were used for lipids and peptides, respectively.

Atomic Force Microscopy (AFM). The influence of Mag2 or Mag-A on the morphology of DMPC and DMPC/DMPG (4 : 1) bilayers were examined by a Nanoscope IV AFM with a Multimode head (Veeco, Santa Barbara, CA, USA) using a vertical engage 'E' scanner. Images were obtained in 20 mM phosphate buffer pH 7.4 *via* taping mode with NSC-36 'B' silicon cantilevers (Micromasch, Tallinn, Estonia) with a nominal force constant of 1.75 N/m. 20 μl of freshly prepared liposome (50 nm) solution was deposited onto freshly cleaved mica and incubated at 40°C for 30 min. After incubation, the surface was rinsed 3 times with buffer at 25°C. The bilayers were then imaged in buffer using the liquid cell with several additions of 15 μl of 10 μM peptide over the supported bilayers. Topographic, phase and amplitude images at a resolution of 512 × 512 were simultaneously obtained using scan frequencies between 0.5–1.5 Hz with typical scan sizes of 5 μm × 5 μm, 2 μm × 2 μm, 1 μm × 1 μm or 500 nm × 500 nm. Minimal force (free oscillating amplitude ~20 nm, setpoint of 60–80%) was used to reduce the mechanical agitation inflicted on the sample. Images were processed with a sequence of plane fitting and offset flattening using either WSxM 4.0 (www.nanotec.es) or Gwyddion 2.29 (www.gwyddion.net) software.

1. Huang, H. W. Molecular mechanism of antimicrobial peptides: the origin of cooperativity. *Biochim Biophys Acta* **1758**, 1292–1302 (2006).
2. Zasloff, M. Antimicrobial peptides of multicellular organisms. *Nature* **415**, 389–395 (2002).
3. Gee, M. L. *et al.* Imaging the action of antimicrobial peptides on living bacterial cells. *Sci Rep* **3**, 1557 (2013).
4. Lee, T. H. *et al.* Real-time quantitative analysis of lipid disordering by aurein 1.2 during membrane adsorption, destabilisation and lysis. *Biochim Biophys Acta* **1798**, 1977–1986 (2010).
5. Rakowska, P. D. *et al.* Nanoscale imaging reveals laterally expanding antimicrobial pores in lipid bilayers. *Proc Natl Acad Sci U S A* **110**, 8918–8923 (2013).
6. Melo, M. N., Ferre, R. & Castanho, M. A. Antimicrobial peptides: linking partition, activity and high membrane-bound concentrations. *Nat Rev Microbiol* **7**, 245–250 (2009).
7. Jackson, M., Mantsch, H. H. & Spencer, J. H. Conformation of magainin-2 and related peptides in aqueous solution and membrane environments probed by Fourier transform infrared spectroscopy. *Biochemistry* **31**, 7289–7293 (1992).
8. Bechinger, B., Zasloff, M. & Opella, S. J. Structure and orientation of the antibiotic peptide magainin in membranes by solid-state nuclear magnetic resonance spectroscopy. *Protein Sci* **2**, 2077–2084 (1993).
9. Matsuzaki, K., Sugishita, K., Fujii, N. & Miyajima, K. Molecular basis for membrane selectivity of an antimicrobial peptide, magainin 2. *Biochemistry* **34**, 3423–3429 (1995).
10. Boggs, J. M. *et al.* Effect of magainin, class L, and class A amphipathic peptides on fatty acid spin labels in lipid bilayers. *Biochim Biophys Acta* **1511**, 28–41 (2001).
11. Tamba, Y. & Yamazaki, M. Single giant unilamellar vesicle method reveals effect of antimicrobial peptide magainin 2 on membrane permeability. *Biochemistry* **44**, 15823–15833 (2005).
12. Ludtke, S. J. *et al.* Membrane pores induced by magainin. *Biochemistry* **35**, 13723–13728 (1996).
13. Matsuzaki, K. Magainins as paradigm for the mode of action of pore forming polypeptides. *Biochim Biophys Acta* **1376**, 391–400 (1998).
14. Matsuzaki, K. *et al.* Relationship of membrane curvature to the formation of pores by magainin 2. *Biochemistry* **37**, 11856–11863 (1998).
15. Dathe, M., Nikolenko, H., Meyer, J., Beyermann, M. & Bienert, M. Optimization of the antimicrobial activity of magainin peptides by modification of charge. *FEBS Lett* **501**, 146–150 (2001).
16. Tachi, T., Epand, R. F., Epand, R. M. & Matsuzaki, K. Position-dependent hydrophobicity of the antimicrobial magainin peptide affects the mode of peptide-lipid interactions and selective toxicity. *Biochemistry* **41**, 10723–10731 (2002).
17. Dempsey, C. E., Hawrani, A., Howe, R. A. & Walsh, T. R. Amphipathic antimicrobial peptides–from biophysics to therapeutics? *Protein Pept Lett* **17**, 1334–1344 (2010).
18. Domadia, P. N., Bhunia, A., Ramamoorthy, A. & Bhattacharjya, S. Structure, interactions, and antibacterial activities of MSI-594 derived mutant peptide MSI-594F5A in lipopolysaccharide micelles: role of the helical hairpin conformation in outer-membrane permeabilization. *J Am Chem Soc* **132**, 18417–18428 (2010).
19. Chen, H. C., Brown, J. H., Morell, J. L. & Huang, C. M. Synthetic magainin analogues with improved antimicrobial activity. *FEBS Lett* **236**, 462–466 (1988).
20. Richards, R. C., O'Neil, D. B., Thibault, P. & Ewart, K. V. Histone H1: an antimicrobial protein of Atlantic salmon (Salmo salar). *Biochem Biophys Res Commun* **284**, 549–555 (2001).
21. Hicks, R. P. *et al.* Comparison of the conformation and electrostatic surface properties of magainin peptides bound to sodium dodecyl sulfate and dodecylphosphocholine micelles. *Biopolymers* **68**, 459–470 (2003).
22. Epand, R. F., Raguse, T. L., Gellman, S. H. & Epand, R. M. Antimicrobial 14-helical beta-peptides: potent bilayer disrupting agents. *Biochemistry* **43**, 9527–9535 (2004).
23. Matsuzaki, K. *et al.* Orientational and aggregational states of magainin 2 in phospholipid bilayers. *Biochemistry* **33**, 3342–3349 (1994).
24. Mecke, A., Lee, D. K., Ramamoorthy, A., Orr, B. G. & Banaszak Holl, M. M. Membrane thinning due to antimicrobial peptide binding: an atomic force microscopy study of MSI-78 in lipid bilayers. *Biophys J* **89**, 4043–4050 (2005).
25. Imura, Y., Choda, N. & Matsuzaki, K. Magainin 2 in action: distinct modes of membrane permeabilization in living bacterial and mammalian cells. *Biophys J* **95**, 5757–5765 (2008).
26. Fernandez, D. I., Lee, T.-H., Sani, M.-A., Aguilar, M.-I. & Separovic, F. Proline Facilitates Membrane Insertion of the Antimicrobial Peptide Maculatin 1.1 via Surface Indentation and Subsequent Lipid Disordering. *Biophysical journal* **104**, 1495–1507 (2013).
27. Hirst, D. J., Lee, T. H., Swann, M. J. & Aguilar, M. I. Combined mass and structural kinetic analysis of multistate antimicrobial peptide-membrane interactions. *Anal Chem* **85**, 9296–9304 (2013).
28. Hirst, D. J. *et al.* Effect of acyl chain structure and bilayer phase state on binding and penetration of a supported lipid bilayer by HPA3. *Eur Biophys J* **40**, 503–514 (2011).

29. Lee, T. H. *et al.* The membrane insertion of helical antimicrobial peptides from the N-terminus of Helicobacter pylori ribosomal protein L1. *Biochim Biophys Acta* **1798**, 544–557 (2010).
30. Yang, X. & Walsh, P. N. An ordered sequential mechanism for Factor IX and Factor IXa binding to platelet receptors in the assembly of the Factor X-activating complex. *Biochem J* **390**, 157–167 (2005).
31. Fernandez, D. I. *et al.* Structural effects of the antimicrobial peptide maculatin 1.1 on supported lipid bilayers. *European Biophysics Journal* **42**, 47–59 (2013).
32. Haney, E. F., Nathoo, S., Vogel, H. J. & Prenner, E. J. Induction of non-lamellar lipid phases by antimicrobial peptides: a potential link to mode of action. *Chem Phys Lipids* **163**, 82–93 (2010).
33. Gottler, L. M. & Ramamoorthy, A. Structure, membrane orientation, mechanism, and function of pexiganan–a highly potent antimicrobial peptide designed from magainin. *Biochim Biophys Acta* **1788**, 1680–1686 (2009).
34. Ramamoorthy, A., Thennarasu, S., Lee, D. K., Tan, A. & Maloy, L. Solid-state NMR investigation of the membrane-disrupting mechanism of antimicrobial peptides MSI-78 and MSI-594 derived from magainin 2 and melittin. *Biophys J* **91**, 206–216 (2006).
35. Nguyen, K. T., Le Clair, S. V., Ye, S. & Chen, Z. Molecular interactions between magainin 2 and model membranes in situ. *J Phys Chem B* **113**, 12358–12363 (2009).
36. Yang, P., Ramamoorthy, A. & Chen, Z. Membrane orientation of MSI-78 measured by sum frequency generation vibrational spectroscopy. *Langmuir* **27**, 7760–7767 (2011).
37. Melo, M. N. *et al.* Prediction of antibacterial activity from physicochemical properties of antimicrobial peptides. *PLoS One* **6**, e28549 (2011).
38. Garidel, P. & Blume, A. Miscibility of phosphatidylethanolamine-phosphatidylglycerol mixtures as a function of pH and acyl chain length. *Eur Biophys J* **28**, 629–638 (2000).
39. Iraolagoitia, X. L. & Martini, M. F. Ca(2+) adsorption to lipid membranes and the effect of cholesterol in their composition. *Colloids Surf B Biointerfaces* **76**, 215–220 (2010).
40. Ouberai, M. M. *et al.* alpha-Synuclein senses lipid packing defects and induces lateral expansion of lipids leading to membrane remodeling. *J Biol Chem* **288**, 20883–20895 (2013).
41. Chen, Y. H., Yang, J. T. & Chau, K. H. Determination of the helix and beta form of proteins in aqueous solution by circular dichroism. *Biochemistry* **13**, 3350–3359 (1974).
42. Hall, K., Lee, T. H. & Aguilar, M. I. The role of electrostatic interactions in the membrane binding of melittin. *Journal of Molecular Recognition* **24**, 108–118 (2011).
43. Hall, K., Lee, T.-H., Daly, N. L., Craik, D. J. & Aguilar, M.-I. Gly^6 of kalata B1 is critical for the selective binding to phosphatidylethanolamine membranes. *Biochimica et Biophysica Acta (BBA)-Biomembranes* **1818**, 2354–2361 (2012).
44. Mozsolits, H., Lee, T.-H., Clayton, A., Sawyer, W. & Aguilar, M. The membrane-binding properties of a class A amphipathic peptide. *European biophysics journal* **33**, 98–108 (2004).
45. Mozsolits, H. *et al.* Electrostatic and Hydrophobic Forces Tether the Proximal Region of the Angiotensin II Receptor (AT1A) Carboxyl Terminus to Anionic Lipids. *Biochemistry* **41**, 7830–7840 (2002).
46. Mozsolits, H., Wirth, H., Werkmeister, J. & Aguilar, M. Analysis of antimicrobial peptide interactions with hybrid bilayer membrane systems using surface plasmon resonance. *Biochimica et Biophysica Acta, Biomembranes* **1512**, 64–76 (2001).
47. Mashaghi, A., Swann, M., Popplewell, J., Textor, M. & Reimhult, E. Optical anisotropy of supported lipid structures probed by waveguide spectroscopy and its application to study of supported lipid bilayer formation kinetics. *Anal Chem* **80**, 3666–3676 (2008).
48. Cross, G. H. *et al.* The metrics of surface adsorbed small molecules on the Young's fringe dual slab waveguide interferometer. *J Phys D* **37**, (2004).

Acknowledgments

The financial support of the Faculty of Medicine, Nursing & Health Sciences, Monash University, ATA Scientific, the Australian Research Council, the Potter Foundation, the National Heart Foundation and the European Union Framework Project 7 ASMENA is gratefully acknowledged.

Author contributions

K.H. and T.H.L. designed and performed experiments. K.H., T.H.L., A.I.M. and M.I.A. analysed data. K.H., T.H.L. and A.I.M. prepared figures and K.H., T.H.L., A.I.M., M.S. and M.I.A. wrote and reviewed the manuscript.

Additional information

Supplementary information accompanies this paper at http://www.nature.com/scientificreports

Competing financial interests: Dr Marcus Swann is an employee of Fairfeld, Biolin Scientific, and an inventor of the DPI technology used in this submission.

How to cite this article: Hall, K., Lee, T.-H., Mechler, A.I., Swann, M.J. & Aguilar, M.-I. Real-time Measurement of Membrane Conformational States Induced by Antimicrobial Peptides: Balance Between Recovery and Lysis. *Sci. Rep.* **4**, 5479; DOI:10.1038/srep05479 (2014).